Supporting Information

Fig. S1. The living brain coral (*Diploria labyrinthiformis*) cored for this study. The diameter of this coral is ~1 m.

www.pnas.org/cgi/doi/10.1073/pnas.1801049115

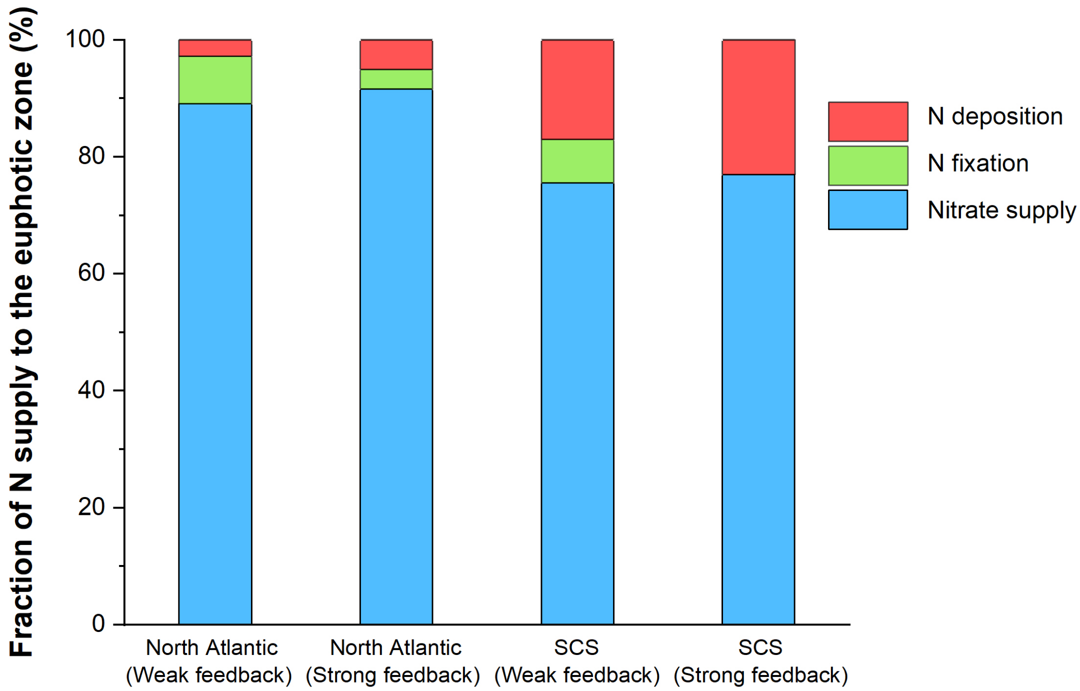

Fig. S2. Comparison of the relative fractions of N supply to the euphotic zone in the subtropical North Atlantic and South China Sea for the year 2000 following the isotope mixing approach in (1). The "weak feedback" scenarios assume a constant N fixation rate over the study periods while the "strong feedback" scenarios include a decrease of N fixation rate as AAN deposition rate increases (in a one-to-one proportion). In the subtropical North Atlantic, the upward nitrate supply has been estimated to be 0.5-0.8 mol N m^{-2} $year^{-1}$ (2-4). The N fixation rate estimation in the subtropical North Atlantic ranges from 0.01 to 0.08 mol N m^{-2} $year^{-1}$ (5-7), representing 2-14% of total N supply to the euphotic zone. Here we use an intermediate N fixation rate in our calculation, representing 8% of total N supply. Regardless of the N fixation rates used in this calculation, across all scenarios, AAN deposition contributes less than 5% of total N supply to the euphotic zone.

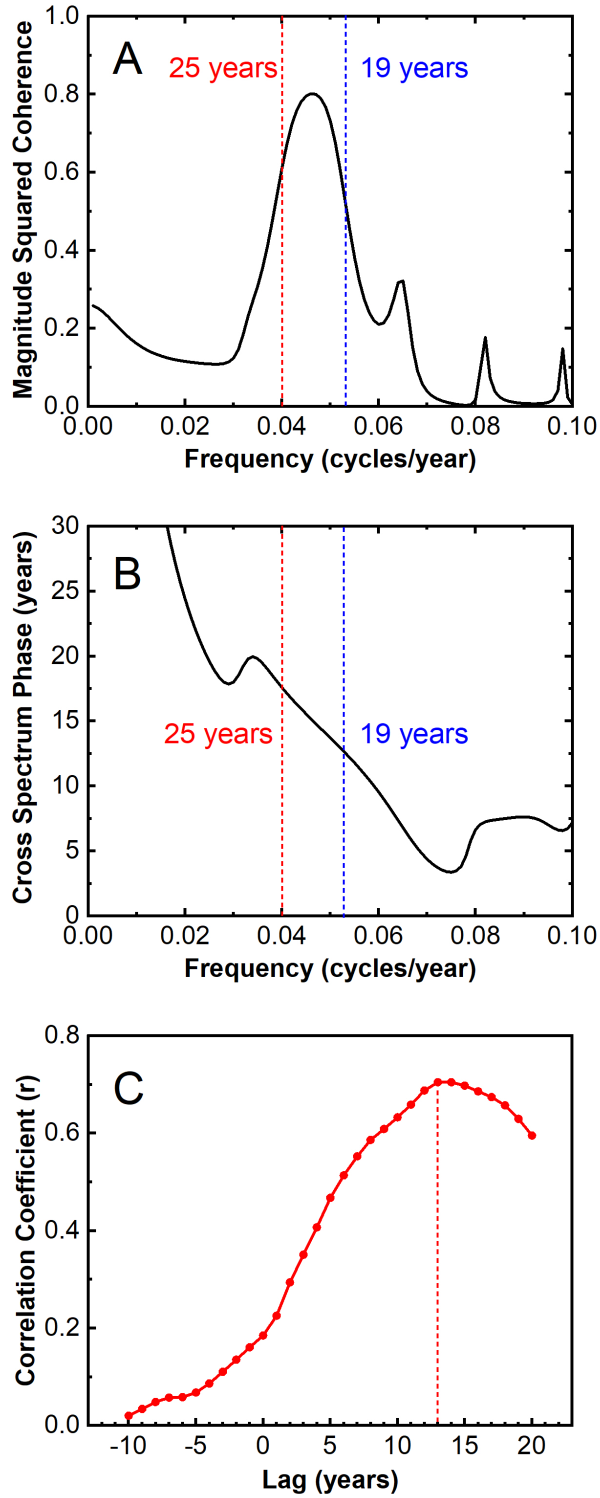

Fig. S3. Magnitude-squared coherence (A), cross spectrum phase (B), and time-dependent correlation coefficients (C) between the smoothed CS-δ^{15}N and NAO records in Fig. 3. At the frequency ranges of 1/25 to 1/19 (red and blue dashed lines), the magnitude-squared coherence (A) has values higher than 0.7, indicating high correlation between CS-$\delta^{15}N$ and NAO. Correspondingly, the cross spectrum phase analysis (B) shows that NAO leads CS-$\delta^{15}N$ by 12-17 years at the frequency ranges of 1/25 to 1/19. Consistent with the cross spectrum phase, the time-dependent correlation analysis (C) shows maximum correlation (r= 0.7) between CS-$\delta^{15}N$ and NAO when NAO leads CS-$\delta^{15}N$ by 13 years.

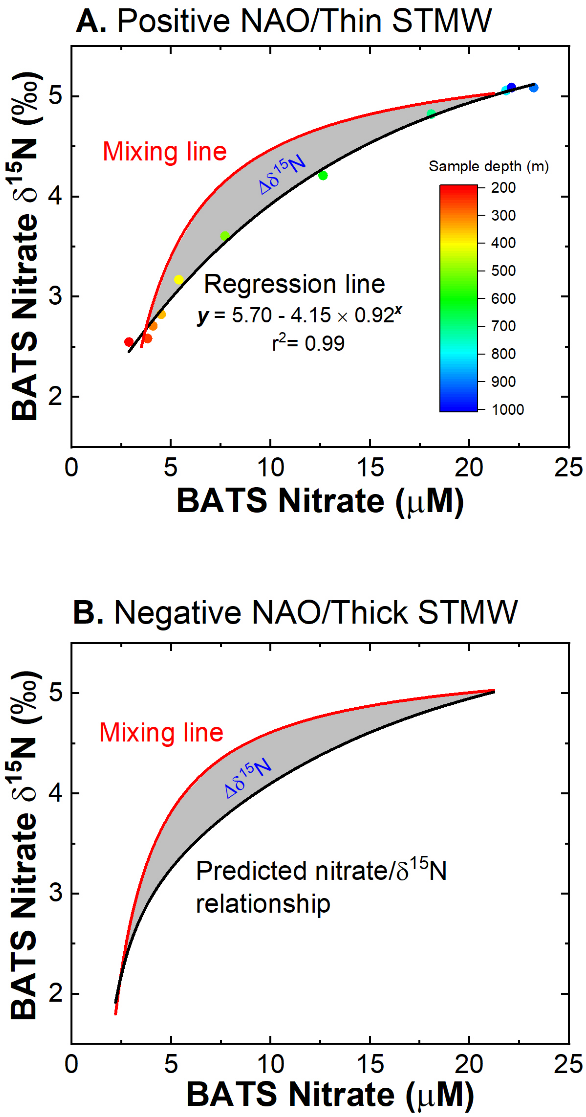

Fig. S4. Calculation of the $[NO_3^-]/\delta^{15}N$ relationship in the Sargasso Sea following strong Subtropical Mode Water formation during a negative phase of NAO. (A) Measured nitrate concentration and $\delta^{15}N$ at BATS following a period of positive NAO. The circles (color coded by depth) are based on data averaged over 18 cruises at BATS(8) since 2005. The red line is the mixing trend between the water in the shallow thermocline at 200m ($[NO_3^-]$ = 3.5μM, $\delta^{15}N$ = 2.5‰) and the water at the base of the thermocline at 1000m ($[NO_3^-]$ = 21.2μM, $\delta^{15}N$ = 5.0‰). The black line is the regression line fitted with an exponential function. The gray area indicates the difference between the mixing line and the regression line, which is caused by the remineralization of low-$\delta^{15}N$ newly fixed N occurring throughout the full depth of thermocline(9). (B) Calculated $[NO_3^-]/\delta^{15}N$ relationship at BATS after a period of strong STMW formation. The red line is the mixing trend between the water at 200m ($[NO_3^-]$ = 2.2μM, $\delta^{15}N$ = 1.8‰) and the water at 1000m ($[NO_3^-]$ = 21.2μM, $\delta^{15}N$ = 5.0‰) when a strong STMW layer appears at BATS. The nitrate $\delta^{15}N$ at 200m with STMW is based on the observed CS-$\delta^{15}N$ in the 1980s (i.e., CS-$\delta^{15}N$ suggests that the nitrate $\delta^{15}N$ at 200m was 0.7‰ lower than the modern condition). The $[NO_3^-]/\delta^{15}N$ relationship with a thick STMW layer is calculated by subtracting the gray area in (A) from the mixing line in (B). This $[NO_3^-]/\delta^{15}N$ relationship is then used to estimate the depth profile of nitrate $\delta^{15}N$ during a negative phase of NAO in Fig. S5.

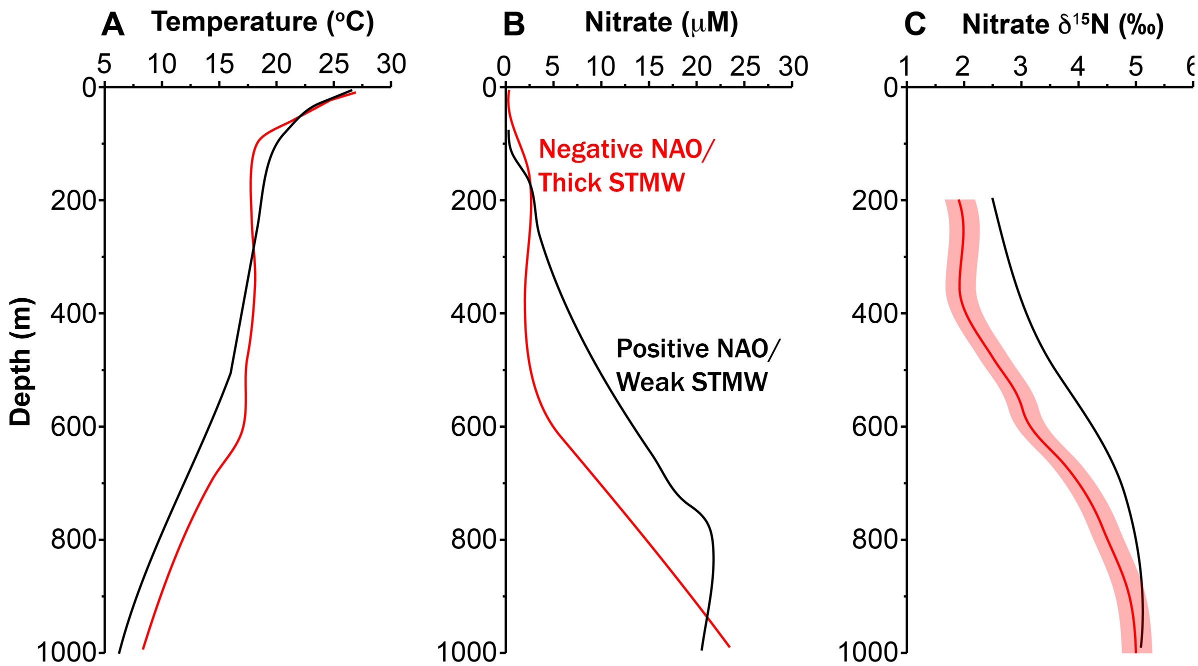

Fig. S5. Depth profiles of temperature, nitrate concentrations and nitrate $\delta^{15}N$ near Bermuda as in Fig. 4 during phases of positive (black lines) and negative (red lines) NAO. The measured temperature (A) and nitrate concentration (B) depth profiles are from a previous study(10). The nitrate $\delta^{15}N$ (C) depth profile under positive NAO is from Fig. 1, while the nitrate $\delta^{15}N$ depth profile under negative NAO is calculated from the $[NO_3^-]/\delta^{15}N$ relationship in Fig. S4. The shaded area is the error (1σ) associated with this calculation based on Monte-Carlo simulations.

References

1. Ren H, et al. (2017) 21st-century rise in anthropogenic nitrogen deposition on a remote coral reef. *Science* 356(6339):749–752.

2. Jenkins WJ (1988) Nitrate Flux Into the Euphotic Zone Near Bermuda. *Nature* 331(6156):521–523.

3. Jenkins WJ, Doney SC (2003) The subtropical nutrient spiral. *Global Biogeochem Cycles* 17(4):1110.

4. Stanley RHR, Jenkins WJ, Doney SC, Lott DE III (2015) The 3He flux gauge in the Sargasso Sea: a determination of physical nutrient fluxes to the euphotic zone at the Bermuda Atlantic Time-series Site. *Biogeosciences* 12(17):5199–5210.

5. Gruber N, Sarmiento JL (1997) Global patterns of marine nitrogen fixation and denitrification. *Global Biogeochem Cycles* 11(2):235–266.

6. Marconi D, et al. (2017) Tropical Dominance of N2 Fixation in the North Atlantic Ocean. *Global Biogeochem Cycles* 31(10):1608–1623.

7. Singh A, Lomas MW, Bates NR (2013) Revisiting N2 fixation in the North Atlantic Ocean: Significance of deviations from the Redfield Ratio, atmospheric deposition and climate variability. *Deep Sea Res Part II Top Stud Oceanogr* 93:148–158.

8. Fawcett SE, Ward BB, Lomas MW, Sigman DM (2015) Vertical decoupling of nitrate assimilation and nitrification in the Sargasso Sea. *Deep Sea Res Part I Oceanogr Res Pap* 103:64–72.

9. Marconi D, et al. (2015) Nitrate isotope distributions on the US GEOTRACES North Atlantic cross-basin section: Signals of polar nitrate sources and low latitude nitrogen cycling. *Mar Chem* 177:143–156.

10. Palter JB, Lozier MS, Barber RT (2005) The effect of advection on the nutrient reservoir in the North Atlantic subtropical gyre. *Nature* 437(7059):687–692.